frontiers in Marine Science

ORIGINAL RESEARCH
published: 23 March 2018
doi: 10.3389/fmars.2018.00096

TAG Plume: Revisiting the Hydrothermal Neodymium Contribution to Seawater

Torben Stichel[1]†, Katharina Pahnke[2], Brian Duggan[3], Steven L. Goldstein[4], Alison E. Hartman[4], Ronja Paffrath[2] and Howie D. Scher[3]*

[1] School of Ocean and Earth Sciences, University of Hawaii at Manoa, Honolulu, HI, United States, [2] Max Planck Research Group for Marine Isotope Geochemistry, Institute for Chemistry and Biology of the Marine Environment, University of Oldenburg, Oldenburg, Germany, [3] Department of Earth and Ocean Sciences, University of South Carolina, Columbia, SC, United States, [4] Lamont-Doherty Earth Observatory and Department of Earth and Environmental Sciences, Columbia University, Palisades, NY, United States

Edited by:
Johan Schijf,
Chesapeake Biological Laboratory,
United States

Reviewed by:
Hiroshi Amakawa,
Japan Agency for Marine-Earth
Science and Technology, Japan
Kazuyo Tachikawa,
UMR7330 Centre Européen de
Recherche et D'enseignement de
Géosciences de L'environnement
(CEREGE), France

***Correspondence:**
Torben Stichel
torben.stichel@awi.de

†Present Address:
Torben Stichel,
Alfred Wegener Institute, Helmholtz
Centre for Polar and Marine Research,
Bremerhaven, Germany

Specialty section:
This article was submitted to
Marine Biogeochemistry,
a section of the journal
Frontiers in Marine Science

Received: *15 December 2017*
Accepted: *07 March 2018*
Published: *23 March 2018*

Citation:
Stichel T, Pahnke K, Duggan B, Goldstein SL, Hartman AE, Paffrath R and Scher HD (2018) TAG Plume: Revisiting the Hydrothermal Neodymium Contribution to Seawater. Front. Mar. Sci. 5:96. doi: 10.3389/fmars.2018.00096

We present results on the distribution of ε_{Nd} and [Nd] from the TAG hydrothermal vent field and adjacent locations collected during the GEOTRACES GA03 cruise in October 2011. Our results show that Nd isotopes directly below and above the plume do not significantly deviate from average NADW ($\varepsilon_{Nd} = -12.3 \pm 0.2$). Within the plume, however, isotope values are shifted slightly toward more radiogenic values up to $\varepsilon_{Nd} = -11.4$. Interestingly at the same time a significant decrease in [Nd] along with rare earth element (REE) fractionation is observed, indicating enhanced scavenging within the plume despite the change in Nd isotopes. Elemental concentrations of Nd are reduced by 19.6–18.5 pmol/kg, coinciding with the maximum increase of mantle derived helium (xs^3He) from 0.203 to 0.675 fmol/kg, resulting in an average 1.8 pmol/kg decrease in [Nd] relative to an expected linear increase with depth. The inventory loss of Nd within the plume sums up to 614 nmoles/m^2, or 6%, if a continuous increase of [Nd] with depth is assumed. Compared to BATS and the western adjacent station USGT11-14, the local inventory loss is even higher at 10%. The tight relationship of xs^3He increase and [Nd] decrease allows us to estimate scavenging rates at TAG suggesting 40 mol/year are removed within the TAG plume. A global estimate using power output along ocean ridges yields an annual Nd removal of 3.44×10^6 mol/year, which is about 71% of riverine and dust flux combined or 6–8% of the estimated global flux of Nd into the ocean. The change in Nd isotopic composition of up to 0.7 more radiogenic ε_{Nd} values suggests an exchange process between hydrothermally derived particles and seawater in which during the removal process an estimated 1.1 mol/year of hydrothermal Nd is contributed to the seawater at the TAG site. This estimate is only 0.1% of the global Nd signal added to the ocean by boundary exchange processes at ocean margins, limiting the ability of changing the Nd isotopic composition on a global scale in contrast to the more significant estimated sink of elemental Nd in hydrothermal plumes from this study.

Keywords: neodymium isotopic compositions, GEOTRACES, hydrothermal plume, rare earth elements, seawater, TAG

INTRODUCTION

The isotopic composition of the rare earth elements (REE) neodymium (Nd), expressed in $\varepsilon_{Nd} = \{(^{143}Nd/^{144}Nd)_{sample}/(^{143}Nd/^{144}Nd)_{CHUR}-1\} \times 10^4$, with CHUR = 0.512638 (Jacobsen and Wasserburg, 1980), has been widely used as water mass tracer for modern and paleo ocean circulation patterns (Piepgras and Wasserburg, 1982; Goldstein and Hemming, 2003; Piotrowski et al., 2004; Pena and Goldstein, 2014). Despite continued investigation, the sources and sinks in the Nd cycle are complicated to quantify: Rivers and dust input only contribute a relatively small amount of Nd into the ocean and influence mostly the upper mixed layer with $\sim 4.3 \times 10^6$ moles/year (Goldstein and Jacobsen, 1987; Tachikawa et al., 1999, 2003; Arsouze et al., 2009; Rempfer et al., 2011), an additional "missing flux" of 3.8 to 5.5×10^7 mol/year (Tachikawa et al., 2003; Rempfer et al., 2011) is needed to yield an oceanic residence time short enough to explain the heterogeneous distribution of ε_{Nd} in seawater (Goldstein and Hemming, 2003; Tachikawa et al., 2003; Arsouze et al., 2009). The missing flux has been identified as an exchange process, which enables decoupling of Nd isotope composition from Nd concentration (Lacan and Jeandel, 2005; Arsouze et al., 2007, 2009). Recently, the role of ocean margins has received particular attention, as they are a principle player in the global marine cycle of trace elements and their isotopes (TEI) (Lacan and Jeandel, 2001; Jeandel and Oelkers, 2015; Rousseau et al., 2015). From these and other studies, it arose that shelf sediments are a key source and sink of TEI. A more complex source-sink interplay has been invoked for hydrothermal activity and their associated plume dispersion in the deep ocean. While for iron (Fe) (Klunder et al., 2011; Conway and John, 2014; Resing et al., 2015) or manganese (Mn) (Middag et al., 2010; Hatta et al., 2015), hydrothermal activities are an important source, REE are scavenged when hydrothermal fluid mixes with seawater (Klinkhammer et al., 1983; German et al., 1991; Elderfield and Schultz, 1996). In addition, a potential influence of hydrothermal activity on the marine Nd isotopic composition has not been documented yet. One of the most recent studies in the Southeast Pacific Ocean has already suggested that the deep water Nd isotopic composition is influenced by hydrothermal activity (Jeandel et al., 2013). These authors observed an ε_{Nd} increase from −6 in the Southeastern Pacific, typical for water masses of Southern Ocean origin (Carter et al., 2012; Grasse et al., 2012; Stichel et al., 2012; Basak et al., 2015), to −3.7, which was interpreted as potential influence from the East Pacific Rise. However, REE patterns did not show any difference from the other samples in that profile. The scarcity of available combined REE and ε_{Nd} data from hydrothermal plumes has so far limited the study of the impact of hydrothermal activity in geochemical models to the Nd cycle, whereas such systems were not included in previous modeling studies of the global seawater ε_{Nd} distribution (Jones et al., 2008; Siddall et al., 2008; Arsouze et al., 2009; Rempfer et al., 2011).

Here we present for the first time a coupled profile of REE concentrations and Nd isotopic composition within the Trans-Atlantic Geotraverse (TAG) hydrothermal plume, one of the most intensely studied hydrothermal sites. We will compare the TAG profile with stations in the West Atlantic, such as the Bermuda Atlantic Time Series (BATS: USGT11-10 and Pahnke et al., 2012) and an adjacent station west of the vent field (USGT11-14) to determine changes in the Nd budget caused by hydrothermal plumes (**Figure 1**). The three profiles were sampled along the US-GEOTRACES North Atlantic Zonal Transect (NAZT). The TAG station and USGT11-14 are located within the North Atlantic Gyre between the Gulf Stream and North Atlantic Drift (NAD) in the north and the North Equatorial Current (NEC) in the south. Station BATS is located at the western edge of the North Atlantic Gyre, where the Deep Western Boundary Current (DWBC) transports North Atlantic Deep Water (NADW) to the south (**Figure 1**). The presence of the hydrothermal plume at TAG is indicated by a significant increase in primordial He (δ^3He, Jenkins et al., 2015a). In this study, we will use this enrichment in δ^3He, expressed in excess He (xs^{3}He), to identify the extent of the plume, referring to all samples with this enrichment as "within the plume."

METHODS

Samples were collected during the second leg of the US-GEOTRACES GA03 North Atlantic Zonal Transect (NAZT) on the R/V Knorr (KN204-1). The TAG station was sampled Nov. 28 2011 with 11 consecutive CTD casts. Neodymium and other REE concentrations, Nd isotopes and He isotopes were measured from the same cast and bottles. Sample preparation for Nd and Nd isotopes is described in Stichel et al. (2015). Samples were collected in 10 L Niskin bottles mounted on a stainless steel CTD rosette (Conductivity, Temperature, Depth) with additional sensors for beam attenuation and fluoresence. Sub-samples of about 5 L were filtered through AcroPak500 (0.8/0.45 μm) filter cartridges into acid-cleaned pre-weighed LDPE collapsible containers and acidified to pH <2 with 2 mL 6 M HCl (quartz distilled, for all mineral acids) per L seawater. In the home laboratory sub-samples were weighed and an enriched ^{146}Nd spike was added gravimetrically to yield an optimum $^{146}Nd/^{142}Nd$ close to 1. Sub-samples were pre-concentrated by adjusting the pH to ∼3.5 and successively pumping through C18 cartridges (waters, WAT051910) loaded with 350 μL Bis(2-ethylhexyl) hydrogen phosphate (HDEHP, CAS:298-07-7) at 20 mL/min. Barium and remaining sea salts were eluted with 5 mL 0.01 M HCl and REEs were collected with 30 mL 6 M HCl. Prior to pre-concentration the loaded cartridges were cleaned with 2 mL 6 M HCl followed by a rinse with MilliQ water (18.2 MΩcm) until pH settled to 5. The eluted REE solution was dried down and 600 μL aqua regia was added to oxidize organic compounds followed by an evaporation step. The residual was dried down again twice using 1 mL 1 M HNO_3. The final sample was taken up in 0.5 mL 1 M HNO_3 and loaded onto a 100 μL TRU-resin bed (Eichrom, 100–150 μm bead size). Further elution of 5 resin volumes 1 M HNO_3 removed Ca, Sr and remaining Ba. Light REE were collected with 4 resin volumes of 1 M HCl. Purification of Nd was achieved using Teflon distilled 0.2 M alpha- hydroxyisobutyric acid (Alpha-HIBA) adjusted to a pH of 4.5 on ∼700 μL of AG50W-X8 (200–400 mesh) resin. Procedural blanks (onboard

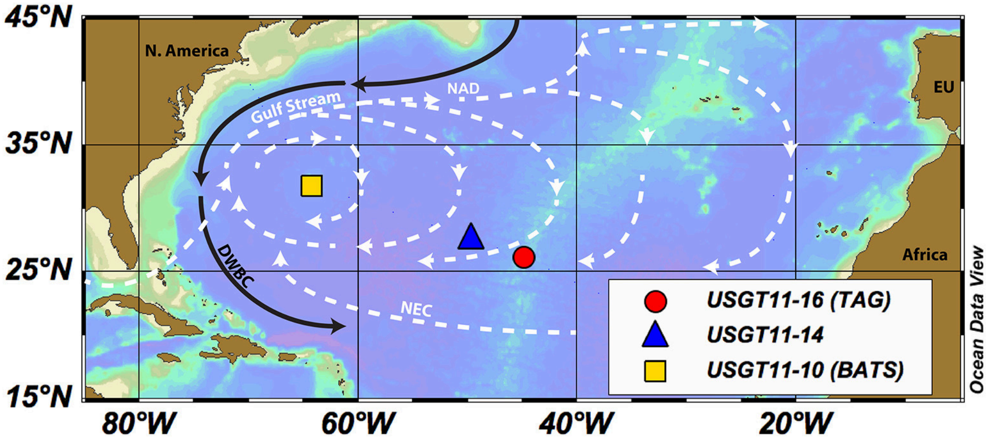

FIGURE 1 | Study area with sampled locations USGT11-10 (BATS, yellow square), USGT11-14 (blue triangle), and USGT11-16 (TAG, red circle). Major currents of the North Atlantic Gyre are illustrated as surface currents in dashed white lines (Gulf Stream, North Atlantic Drift, NAD and North Equatorial Current, NEC) and the Deep Western Boundary Current (DWBC, black line). The figure is designed with ODV® software (Schlitzer, 2016a).

acidified MilliQ water) showed a negligible amount of Nd of <1.5% of the smallest sample size.

Isotopic composition of TAG was measured on a Thermal Ionization Mass Spectrometer (TIMS, VG-Sector) as NdO^+ using 1 μL silica gel as activator (see Stichel et al. (2015) for details) at University of Hawaii yielding an external error of ±0.2 ε_{Nd}, 2SD with $n = 29$. Isotopic composition of USGT11-10 and USGT11-14 was measured using a Thermo Neptune-Plus Multi-Collector ICP-MS at Lamont-Doherty Earth Observatory (LDEO) and University of South Carolina (USC), respectively. At LDEO, a JNdi-1 Nd standard was measured before and after every sample and for three analysis periods yielded an average external error of ±0.3 ε_{Nd}, 2SD, with $n = 83$. At USC, a JNdi-1 standard was measured every four samples with an aimed intensity of 2.5 V on ^{145}Nd. The resulting average external error of ^{143}Nd/^{144}Nd was ±0.4 ε_{Nd}, 2SD, $n = 53$.

All three labs corrected for internal mass fractionation using ^{146}Nd/^{144}Nd $= 0.7219$ in an exponential mass fractionation law and their respective biases from the accepted value of ^{143}Nd/^{144}Nd $= 0.512115$ (Tanaka et al., 2000) for the JNdi-1 Nd standard.

Rare earth elements concentrations were measured at the University of Oldenburg using an offline seaFAST isotope dilution ICP-MS method described in Behrens et al. (2016). The method is intercalibrated with three other laboratories and agrees within analytical uncertainty with the intercalibration results from BATS (Pahnke et al., 2012; Behrens et al., 2016). The external reproducibility of the data presented here is <4% (RSD) except for La (5%) and Ce (8%).

RESULTS AND DISCUSSION

Vertical and Lateral Distribution of Water Masses at TAG

With a few exceptions, the vertical distribution in **Figure 2** and **Table 1** of Nd concentrations [Nd] and isotopic compositions (ε_{Nd}) in the water column at TAG follows similar patterns as profiles in the West Atlantic (BATS and USGT11-14) and the East Atlantic (e.g., USGT10-05, Stichel et al., 2015 not shown). Surface [Nd] of 15.6 pmol/kg at TAG is slightly elevated and with an isotopic composition of $\varepsilon_{Nd} = -11.3 \pm 0.2$ less radiogenic compared to USGT11-14 (15.1 pmol/kg, $\varepsilon_{Nd} = -8.4 \pm 1.6$), BATS (14 pmol/kg, $\varepsilon_{Nd} = -9.5$ to -9.2, this study and Pahnke et al., 2012) and USGT10-05 (12.5 pmol/kg, $\varepsilon_{Nd} = -9.9$, Stichel et al., 2015), which can be attributed to dust deposits from the extension of the Sahara dust plume (Mahowald et al., 2005). Within the surface layer at TAG, [Nd] decrease to a minimum at 111 m coinciding with the fluorometer potential maximum, suggesting scavenging within the mixed layer by biological productivity (**Figure 2**, **Table 1**). From this minimum in [Nd], an increase from 13.7 to 17.8 pmol/kg at 960 m is attributed to remineralization (Stichel et al., 2015; Lambelet et al., 2016). The sharpest increase in [Nd] is between 111 and 420 m (+3.3 pmol/kg). Within this depth range, ε_{Nd} stays fairly constant with some fluctuations -10.9 ± 1.3 (2SD) and gradually decreases to less radiogenic values of $\varepsilon_{Nd} = -11.9$ at around 1,000 m marking the transition of North Atlantic Central Water (NACW) to NADW. At about 1,500 m, the presence of ~80% Upper Labrador Sea Water (ULSW, Jenkins et al., 2015b) corresponds to the least radiogenic isotope composition of $\varepsilon_{Nd} = -12.8$. Within the Classical Labrador Seawater (CLSW), at 2,100 and 2,990 m, the isotopic composition is more radiogenic and constant at around -12.1 ± 0.1. From 420 m, [Nd] is constant to 2,100 m and increases from 17.5 ± 0.5 to 19.6 pmol/kg at 2,990 m. The typical increase below 2,000 m was documented in other studies in the Atlantic Ocean and most recently, based on high resolution profiles, has been attributed to a combination of increase from particle release and lateral advection of preformed REE along with reversible scavenging (Siddall et al., 2008; Stichel et al., 2015; Lambelet et al., 2016; Zheng et al., 2016). This increasing slope in [Nd] is interrupted by a sudden decrease at 3,184 m, coinciding with the upper

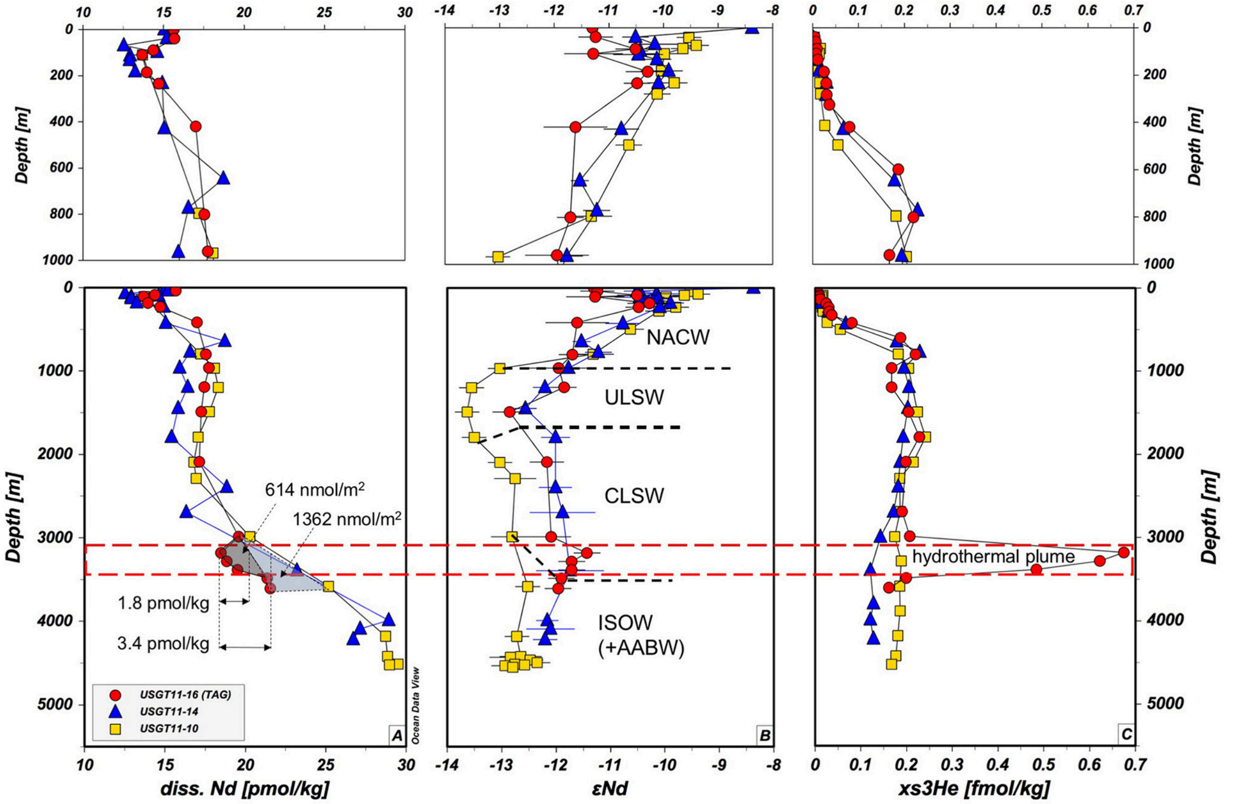

FIGURE 2 | Vertical distribution of dissolved Nd concentration **(A)**, Nd isotopic composition **(B)** and **(C)** mantle derived excess He (xs^{3}He, Jenkins et al., 2015a). Color coding the same as in **Figure 1**. The dashed red line shows the vertical position of the neutrally buoyant hydrothermal plume in the water column. The figure is designed with ODV® software (Schlitzer, 2016a).

extent of the TAG hydrothermal plume (Jenkins et al., 2015a). [Nd] reaches a minimum of 18.48 pmol/kg within the plume, at the depth of maximum mantle derived excess helium (xs^{3}He, Jenkins et al., 2015a). Neodymium isotopes increase by +0.7 at this maximum of xs^{3}He. Below the plume, [Nd] and ε_{Nd} settle back to values that would follow their respective trends above the plume. Using the average [Nd] of two sample depths and multiplying by the vertical distance between these samples, we can calculate the inventory of Nd in the water column by adding up the inventories of each depth interval. If the [Nd] profile followed a simplified but expected linear increase with depth from 2,000 m to the seafloor, the inventory at the plume depth should be 10,493 nmol/m^2. The actual Nd inventory, however, is 9,879 nmol/m^2 due to the lower [Nd] at the TAG plume. The calculated deficit in the Nd inventory between 2,987 m and 3,487 m at TAG station therefore adds up to 614 nmol/m^2 or about 6% (**Figure 2A**). However, compared to stations USGT11-14 at 27.58°N 49.63°W and BATS (USGT11-10), the overall [Nd] at TAG is much lower. Using the [Nd] increase slope of these 2 stations as a reference, the Nd inventory is reduced by roughly 10% (1,362 nmol/m^2) between 2,987 and 3,605 m from the BATS inventory of about 13,837 to 12,474 nmol/m^2 at this depth (**Figure 2**).

TAG Hydrothermal Plume and Its Influence on REE Distribution

At the TAG site, other dissolved REE overall show a similar trend as [Nd] (**Table 2**). However, we observe some fractionation of light and heavy REE (LREE, HREE) within the water column. At about 110 m water depth, where [Nd] is at its lowest value (13.7 pmol/kg, **Figure 2**) the enrichment of PAAS (Taylor and McLennan, 1985) normalized HREE $(Tm+Yb+Lu)_N$ over LREE $(La+Pr+Nd)_N$ is at a maximum value of 5.29 (**Figure 3**), with N for normalization to Post Archaean Australian Shale (PAAS, Taylor and McLennan, 1985). It has been documented in earlier studies that LREE are preferentially scavenged onto particles in the upper water column over HREE (Elderfield and Greaves, 1982) and corroborates that scavenging on particles formed at the chl-max is the main driver of [Nd] decrease. Toward 960 m $HREE_N/LREE_N$ continue their decreasing trend, suggesting release from particles as [Nd] increases in the water column. At the core of upper NADW (1,200 m), these ratios peak at 4.19 and only slightly change up to 4.62 in lower NADW (1,500–2,000 m). Within the TAG plume a preferential scavenging of LREE is observed again. This feature coincides with a strong increase in $Eu/Eu^* = (2 \times Eu_N/\{Sm_N + Gd_N\})$ from 0.965 to 1.22, suggesting the presence of mantle derived Eu

TABLE 1 | Vertical distribution of Nd isotopic composition and concentration, along with xs^{3}He, δ^3He and He concentrations of Jenkins et al. (2015a).

	Depth (m)	^{143}Nd/^{144}Nd	int. error (SEM)	ε_{Nd}^{a}	ext. error (2SD)	[Nd] (pmol/kg)	xs^{3}He^b (fmol/kg)	δ^3He^b (%)	[He]^b (pmol/kg)
USGT11-16	3	0.512058	0.000006	−11.30	0.22	15.6			
26.136°N/44.826°W	40	0.512062	0.000008	−11.24	0.31	15.7	0.005	−1.43	1.68
Depth: 3,810 m	90	0.512099	0.000009	−10.51	0.36	14.4	0.010	−1.21	1.68
	111	0.512060	0.000014	−11.28	0.53	13.7	0.008	−1.31	1.69
	186	0.512111	0.000010	−10.28	0.40	14.0	0.025	−0.62	1.70
	235	0.512101	0.000005	−10.48	0.24	14.7	0.030	−0.43	1.70
	420	0.512043	0.000015	−11.61	0.58	17.0	0.081	1.62	1.74
	801	0.512038	0.000005	−11.70	0.24	17.5	0.220	7.26	1.76
	962	0.512026	0.000015	−11.95	0.58	17.7	0.168	5.02	1.78
	1,194	0.512030	0.000006	−11.85	0.22	17.4	0.168	5.01	1.78
	1,493	0.511979	0.000008	−12.85	0.31	17.3	0.205	6.54	1.77
	2,092	0.512014	0.000008	−12.17	0.31	17.1	0.199	6.23	1.79
	2,987	0.512018	0.000009	−12.09	0.36	19.6	0.207	6.35	1.83
	3,184	0.512052	0.000005	−11.43	0.24	18.5	0.675	24.4	1.86
	3,284	0.512038	0.000005	−11.71	0.24	18.8	0.623	22.5	1.85
	3,384	0.512038	0.000005	−11.71	0.24	19.5	0.484	16.8	1.88
	3,487	0.512028	0.000005	−11.90	0.24	21.4	0.200	6.09	1.83
	3,605	0.512025	0.000005	−11.96	0.24	21.6	0.162	4.66	1.80
USGT11-10	42	0.512149	0.000005	−9.53	0.22		0.004	−1.49	1.68
31.737°N/64.19°W	76	0.512157	0.000004	−9.39	0.22		0.001	−1.59	1.68
Depth: 4,527 m	89	0.512144	0.000005	−9.64	0.22		0.017	−0.94	1.72
	110	0.512126	0.000006	−9.98	0.38	13.7	0.015	−1.06	1.70
	182	0.512124	0.000005	−10.03	0.38		0.012	−1.20	1.70
	233	0.512136	0.000005	−9.80	0.24		0.016	−1.04	1.71
	281	0.512120	0.000004	−10.11	0.24		0.017	−0.98	1.72
	497	0.512093	0.000005	−10.63	0.24		0.055	0.60	1.71
	797	0.512058	0.000003	−11.32	0.38	17.2	0.182	5.71	1.76
	969	0.511970	0.000004	−13.03	0.22	18.1	0.205	6.56	1.77
	1,197	0.511943	0.000006	−13.55	0.22	18.3			
	1,493	0.511939	0.000003	−13.63	0.22	17.8	0.224	7.28	1.78
	1,794	0.511946	0.000005	−13.50	0.22	17.1	0.242	7.97	1.79
	2,094	0.511970	0.000004	−13.03	0.22	16.8	0.215	6.80	1.80
	2,289	0.511984	0.000005	−12.75	0.38	16.9	0.185	5.42	1.84
	2,990	0.511981	0.000004	−12.81	0.38	20.3	0.174	5.10	1.82
	3,584	0.511996	0.000004	−12.52	0.22	25.2	0.185	5.46	1.83
	4,179	0.511986	0.000003	−12.72	0.22	28.7	0.181	4.90	1.94
	4,419	0.511990	0.000003	−12.65	0.38	28.9	0.177	4.87	1.91
	4,431	0.511980	0.000003	−12.84	0.38				
	4,462	0.511998	0.000006	−12.48	0.24				
	4,493	0.512005	0.000005	−12.35	0.24				
	4,511	0.511984	0.000003	−12.76	0.24	29.5			
	4,523	0.511993	0.000004	−12.58	0.22	29.0	0.168	4.88	1.81
	4,531	0.511975	0.000004	−12.94	0.24				
	4,550	0.511982	0.000007	−12.79	0.24				
USGT11-14	1	0.512209	0.000041	−8.37	1.58	15.1			
27.583°N/49.633°W	40	0.512099	0.000006	−10.51	0.24	15.2	0.000	−1.62	1.68
Depth: 4,501 m	69	0.512118	0.000011	−10.15	0.42	12.5	0.002	−1.56	1.69
	99	0.512104	0.000004	−10.42	0.14	14.6	0.010	−1.26	1.70

(Continued)

TABLE 1 | Continued

Depth (m)	^{143}Nd/^{144}Nd	int. error (SEM)	ϵ^{a}_{Nd}	ext. error (2SD)	[Nd] (pmol/kg)	xs^{3}He^b (fmol/kg)	δ^3He^b (%)	[He]^b (pmol/kg)
114	0.512102	0.000012	−10.46	0.45	12.9	0.009	−1.28	1.70
134	0.512119	0.000007	−10.12	0.26	12.9	0.014	−1.09	1.71
184	0.512130	0.000006	−9.90	0.24	13.2	0.031	−0.38	1.71
234	0.512121	0.000005	−10.09	0.19	14.9	0.067	1.11	1.71
429	0.512086	0.000008	−10.77	0.32	15.1	0.179	5.67	1.74
647	0.512047	0.000004	−11.53	0.16	18.7	0.229	7.63	1.76
773	0.512063	0.000006	−11.22	0.24	16.6	0.195	6.19	1.76
965	0.512035	0.000007	−11.77	0.29	15.9	0.206	6.55	1.78
1,196	0.512013	0.000006	−12.20	0.22	16.4			
1,448	0.511994	0.000005	−12.56	0.2	15.8	0.203	6.50	1.77
1,794	0.512022	0.000007	−12.01	0.26	15.4	0.193	5.97	1.79
2,394	0.512022	0.000008	−12.01	0.3	18.8	0.182	5.46	1.81
2,696	0.512029	0.000016	−11.88	0.6	16.3	0.172	5.03	1.81
3,395	0.512036	0.000016	−11.74	0.62	23.2	0.121	2.99	1.81
3,990	0.512015	0.000005	−12.16	0.2	28.9	0.121	2.98	1.82
4,094	0.512018	0.000011	−12.10	0.44	27.2			
4,218	0.512013	0.000006	−12.20	0.22	26.7	0.128	3.28	1.81

[a] *ε_{Nd} = {R/CHUR−1} × 10,000, with R = ^{143}Nd/^{144}Nd and CHUR = 0.512638 (Jacobsen and Wasserburg, 1980).* [b] *Data from Jenkins et al. (2015a).*

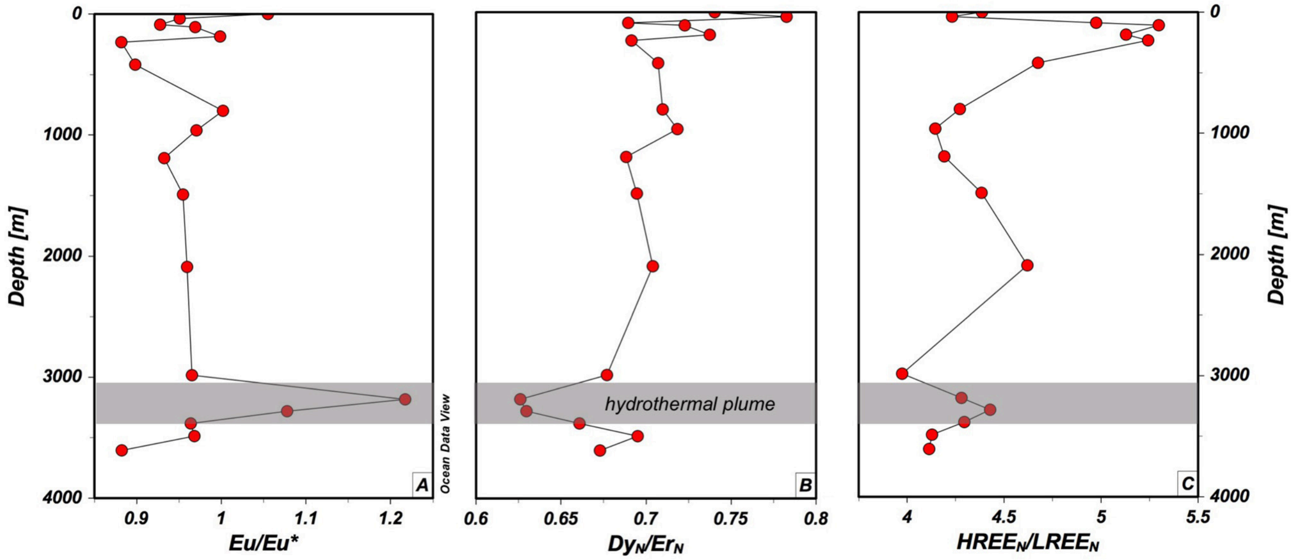

FIGURE 3 | Vertical distribution of Eu/Eu* **(A)**, PAAS (Taylor and McLennan, 1985) normalized Dy/Er **(B)** and HREE (Tm+Yb+Lu) over LREE (La+Pr+Nd) **(C)** and their associated anomalies within the TAG plume at station USGT11-16. The figure is designed with ODV® software (Schlitzer, 2016a).

leached out of basaltic plagioclases, and a moderate decrease from 0.704 to 0.626 in the overall homogenous Dy_N/Er_N at the highest xs^{3}He, indicating the influence of hydrothermal activity on REE (**Figure 3**).

Implications on the Global Nd Cycle

The significant depletion of [Nd] within the hydrothermal plume correlates well with xs^{3}He (Jenkins et al., 2015a), in that high excess He corresponds to low [Nd] and vice versa (**Figure 4A**). The depletion of [Nd] within the TAG plume thus corroborates that hydrothermal activity is a net sink for Nd and other REE (German et al., 1990) and is attributed to the formation of ferrihydrite (Ohnemus and Lam, 2015) co-precipitating REE. With paired He and Nd data available from one hydrothermal plume for the first time, we revisit this scavenging by estimating the annual removal of Nd using an approach suggested in Jenkins et al. (2015a). If we assume a linear increase of Nd with depth below ~2,000 m such as observed at stations USGT11-10

TABLE 2 | REE concentrations and ratios at USGT11-16 (TAG).

Depth	La	Ce	Pr	Nd	Sm	Eu	Gd	Tb	Dy	Ho	Er	Tm	Yb	Lu	Eu/Eu*	$\text{HREE}_N/\text{LREE}_N$	Dy_N/Er_N
(m)							(pmol/kg)								$(2 \times \text{Eu}_N / \{\text{Sm}_N + \text{Gd}_N\})$	$(\{\text{Tm+Yb+Lu}\}_N/\{\text{La+Pr+Nd}\}_N)$	
1	12.9	19.7	3.55	15.7	3.32	0.852	4.05	0.733	6.02	1.27	4.81	0.603	3.95	0.631	1.06	4.39	0.740
40	15.0	17.1	3.53	15.4	3.29	0.859	4.90	0.776	5.53	1.37	4.18	0.631	3.68	0.643	0.951	4.24	0.783
90	13.5	11.9	3.12	13.4	2.94	0.772	4.56	0.722	5.07	1.37	4.35	0.662	3.89	0.649	0.928	4.98	0.690
111	12.5	12.2	2.94	13.4	2.82	0.770	4.36	0.726	5.73	1.27	4.69	0.632	4.24	0.666	0.969	5.29	0.723
186	13.7	19.7	3.01	13.9	2.94	0.798	4.32	0.747	5.96	1.37	4.78	0.657	4.25	0.670	1.00	5.12	0.738
235	14.5	7.60	3.58	14.1	3.34	0.837	5.26	0.842	5.81	1.58	4.97	0.780	4.38	0.745	0.882	5.25	0.692
420	17.2	7.16	3.90	16.3	3.70	0.887	5.29	0.886	6.42	1.56	5.37	0.755	4.76	0.754	0.898	4.70	0.707
801	18.4	2.92	4.06	16.5	3.53	0.885	4.57	0.743	5.28	1.37	4.40	0.682	4.25	0.790	1.00	4.27	0.710
962	21.4	3.18	3.85	17.5	3.37	0.889	4.94	0.722	5.55	1.38	4.57	0.696	4.30	0.817	0.971	4.13	0.719
1,194	22.7	3.67	3.99	18.2	3.39	0.840	4.79	0.767	5.48	1.46	4.71	0.742	4.53	0.867	0.933	4.19	0.688
1,493	22.1	3.49	4.10	16.9	3.28	0.891	5.14	0.756	5.60	1.46	4.77	0.736	4.70	0.892	0.955	4.38	0.695
2,093	22.7	3.31	3.40	16.9	3.03	0.830	4.78	0.666	5.45	1.36	4.58	0.711	4.91	0.907	0.960	4.62	0.704
2,987	26.0	3.75	4.53	19.9	3.43	0.900	5.02	0.742	5.94	1.41	5.19	0.727	5.29	0.920	0.965	3.97	0.677
3,184	25.5	4.38	4.50	18.9	3.32	1.03	4.39	0.739	5.79	1.40	5.47	0.758	5.48	0.977	1.22	4.27	0.626
3,284	25.2	3.53	4.83	17.9	3.65	1.02	4.96	0.810	5.77	1.58	5.42	0.804	5.56	1.02	1.08	4.44	0.630
3,384	26.9	4.40	5.17	18.7	3.77	0.981	5.45	0.819	6.01	1.53	5.38	0.804	5.73	1.07	0.964	4.30	0.661
3,487	25.7	4.96	5.20	19.9	4.30	1.05	5.59	0.866	6.92	1.54	5.89	0.783	5.52	1.03	0.968	4.14	0.695
3,605	28.5	4.26	5.55	20.4	4.29	1.01	6.10	0.955	6.53	1.73	5.74	0.885	5.64	1.07	0.882	4.10	0.673

N = normalized to PAAS (Taylor and McLennan, 1985).

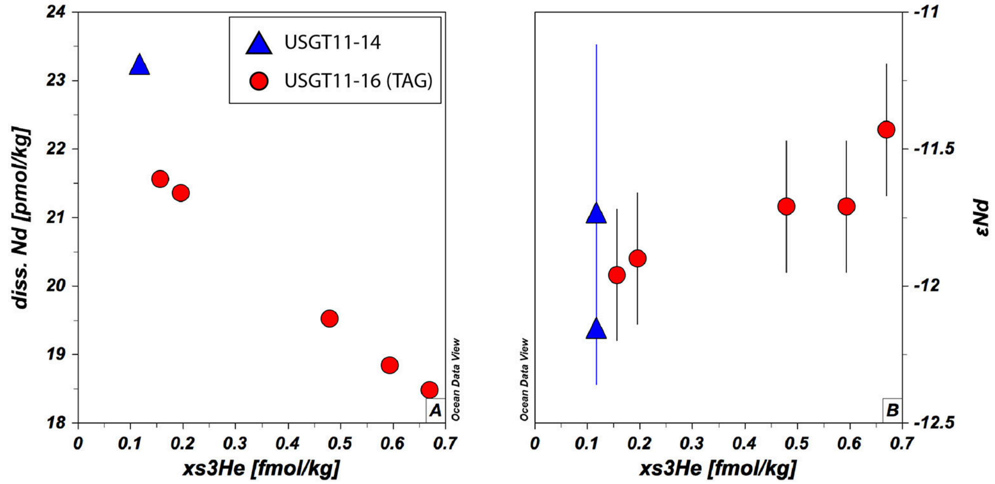

FIGURE 4 | Comparison of xs^{3}He and Nd **(A)** and Nd isotopic composition **(B)** at stations USGT11-14 and TAG between 3,184 and 3,605 m. The figure is designed with ODV® software (Schlitzer, 2016a).

and−14, the minimum average deficit of Nd within the plume is about 1.8 pmol/kg by the shape of the profile of TAG station. Since [Nd] in the plume negatively correlate with xs^{3}He, we can make use of this relationship to estimate Nd scavenging rates based on He fluxes (Jenkins et al., 2015a). The net heat injection into the plume is ~100 J/kg at the plume maximum, which is accompanied by an xs^{3}He anomaly of 0.73 fmol/kg yielding a He:heat ratio of $\sim 7.3 \times 10^{-18}$ mol/J (Jenkins et al., 2015a). Applying this to Nd, we get a Nd:heat ratio -1.8×10^{-14} mol/J. Jenkins et al. (2015a) have used the estimated power output at TAG of 70×10^6 W (Goto et al., 2003) to compute ^{3}He output (15 mmol/year), and based on the tight correlation of He and Nd, we derive a scavenging rate of ~40 mol/year. This local removal of Nd is around 6 orders of magnitude smaller than the annual estimated Nd flux of 3.8–5.5 × 10^7 mol/year (Tachikawa et al., 2003; Rempfer et al., 2011) into the ocean. We are aware that it is difficult and prone to high uncertainty to extrapolate from a single site to a global estimate. However, if we assume similar particle loads in other hydrothermal vent fields, and we extrapolate this He-Nd-heat relationship to a global estimate using a global heat flux of $\sim 3.2 \times 10^{12}$ W along ocean ridges (Stein et al., 2013), the removal rate by hydrothermal activity sums up to $\sim 1.8 \times 10^6$ mol/year. This is about the same as the estimated dust input of 1.8×10^6 mol/year (Rempfer et al., 2011). Again, this is an estimate based on the data this study here provides and it does not take into account factors that could influence hydrothermal plume dispersion such as changing deep ocean currents or differences in ridge geometry. Nevertheless, we argue that the heat flux-He relationship is a valid approach, because the global ^{3}He flux is only slightly higher than recently modeled global ^{3}He fluxes of 450 ± 50 mol/year (Schlitzer, 2016b) compared to 686 mol/year using the values reported in Jenkins et al. (2015a). Our estimate suggests that global hydrothermal activity removes as much Nd from the water column as Nd is released from dust. As mentioned earlier, this number is based on Nd deficit within the profile of the TAG station. If we use the inventory deficit based on the increase of [Nd] with depth at USGT11-10 and −14, which show stronger [Nd] increase with depth, the Nd loss would be about 1.9 times higher, yielding $\sim 3.4 \times 10^6$ mol/year, which is about 71% of riverine and dust flux combined (Goldstein and Jacobsen, 1987; Tachikawa et al., 1999, 2003; Arsouze et al., 2009; Rempfer et al., 2011) or 6–8% of the estimated total global flux (Tachikawa et al., 2003; Rempfer et al., 2011) of Nd into the ocean.

Isotopic Exchange Processes

The [Nd] depletion is accompanied by a slight increase in ε_{Nd} from -12.1 ± 0.4 above to -11.4 ± 0.2 (2SD) at the maximum of the plume (**Figures 2**, **4B** and **Table 1**), suggesting an exchange of Nd isotopes between seawater and a hydrothermal source. While scavenging of REE within a hydrothermal plume by Fe-Mn oxide particles that form as hydrothermal fluids get in contact with oxic seawater has been suggested earlier (German et al., 1990), an isotopic influence on the water column by hydrothermal activity has, to our knowledge, not been documented before. Even though Nd is removed from the water column, the shift in isotopic composition toward more radiogenic values suggests an exchange process that releases radiogenic Nd into the water column to alter its isotopic composition locally. The peak excursion of ~0.7 ε_{Nd} units coincides with the local minimum of [Nd] within the plume. We therefore use the above derived removal flux for Nd (40 mol/year) for a mass balance to calculate the extra Nd needed to explain the shift in the seawater isotopic composition using an end-member ε_{Nd} composition close to that of vent fluids ($\varepsilon_{Nd\,vent} = +11.9$, Mills et al., 2001). We assume here that this end-member composition is found in an unknown hydrothermal flux added to the system (F_{vent}) that is then scavenged within the plume in exchange with ambient seawater. In steady state, the removal of Nd within the plume (F_{plume}, i.e., 40 mol/year) must be further balanced by the addition of seawater (F_{sw}), hence the sum of 'fresh' Nd supplied by seawater and F_{vent} is equal to F_{plume}. The mass balance would then follow this relationship: $\varepsilon_{Ndplume}(F_{plume}) = \varepsilon_{Ndsw}(F_{plume}-F_{vent}) + \varepsilon_{Ndvent}(F_{vent})$. With $\varepsilon_{Ndplume}$ and ε_{Ndsw} representing the isotopic composition within the plume (−11.4) and outside the plume (−12.1), respectively. Solving for F_{vent}, the observed shift in the Nd isotopic composition along with the scavenging of 40 mol/year needs to be balanced by a release of ∼1.1 mol/year Nd to yield the observed isotopic composition within the plume. So the TAG hydrothermal plume is a net sink for Nd and REE in general, however, by isotopic exchange processes the Nd isotopic composition of seawater is altered toward more radiogenic values relative to surrounding water masses. If we assume similar exchange processes in other hydrothermal systems, we can estimate a global flux released from hydrothermal systems. This yields 5.2×10^4 mol/year, accounting for only 0.1% of the estimated release (Tachikawa et al., 2003; Rempfer et al., 2011) from boundary exchange. This suggests that the removal of Nd from seawater by hydrothermal vents is about 35–66 times higher than the Nd added to seawater by these systems. This estimate suggests that on a basin wide scale, the influence of a hydrothermally derived Nd isotopic signal is low and limits the ability to change Nd isotopic seawater composition. However, the influence on [Nd] as a sink is noticeable as mentioned in the previous section and should be taken into account in forthcoming modeling estimates of the Nd cycle.

SUMMARY

For the first time a neutrally buoyant hydrothermal plume was sampled for seawater Nd isotopic composition and REE concentrations and compared with xs^{3}He on a GEOTRACES section cruise (GA03). The data show a clear influence of the hydrothermal plume on the REE concentrations and Nd isotopes. Shale (PAAS, Taylor and McLennan, 1985) normalized Eu/Eu*, Dy/Er and HREE (Tm+Yb+Lu) over LREE (La+Pr+Nd) show clear influence within the hydrothermal plume. The presence of mantle derived Eu is indicated by a significant positive Eu/Eu* at the maximum of xs^{3}He. Fractionation of REE is evident by the relative enrichment of HREE over LREE within the plume. This is further corroborated by decreasing Dy_N/Er_N. Elemental concentrations of Nd are reduced by 19.6–18.5 pmol/kg, coinciding with the maximum increase of xs^{3}He from 0.205 to 0.675 fmol/kg, resulting in an average 1.8 pmol/kg decrease in [Nd] relative to an expected linear increase with depth. The inventory loss of Nd within the plume sums up to ∼614 nmol/m^2, or 6%. Compared to BATS and the western adjacent station USGT11-14, the local inventory loss is even higher at 10%. The tight relationship of xsHe^3 increase and [Nd] decrease allows us to estimate scavenging rates at TAG suggesting ∼40 mol/year are removed within the TAG plume. A global estimate using power output of $\sim 3.2 \times 10^{12}$ W along ocean ridges (Stein et al., 2013) yields an annual Nd removal of $\sim 3.4 \times 10^6$ mol/year, which is about 71% of riverine and dust flux combined (Goldstein and Jacobsen, 1987; Tachikawa et al., 1999, 2003; Arsouze et al., 2009; Rempfer et al., 2011) or 6–8% of the estimated total global flux (Tachikawa et al., 2003; Rempfer et al., 2011) of Nd into the ocean. The change in Nd isotopic composition of up to 0.7 more radiogenic ε_{Nd} values suggests an exchange process between hydrothermally derived particles and seawater in which during the removal process an estimated 1.1 mol/year of hydrothermal Nd is contributed to the seawater at the TAG site. This estimate is ∼0.1% of the global Nd signal added to the ocean by boundary exchange processes at ocean margins (Tachikawa et al., 2003; Rempfer et al., 2011), limiting the ability of changing the Nd isotopic composition on a global scale in contrast to the more significant estimated sink of elemental Nd in hydrothermal plumes from this study.

AUTHOR CONTRIBUTIONS

TS wrote the manuscript. KP, SG, and HS wrote the funding proposal. TS, AH, and BD measured Nd isotopic composition and Nd concentration, RP measured REE concentrations.

ACKNOWLEDGMENTS

The authors would like to thank the scientific party and crew of KN204, especially M. Fleisher and C. Hayes for help with cruise preparations, sampling onboard, and sample storage at LDEO. Thanks to the ODF team for help onboard, and the chief-scientists G. Cutter, W. Jenkins, and E. Boyle. W. Jenkins also provided the He data, which was essential for the scope of this paper. Thanks to D. Vonderhaar, D. Pyle (both UH), L. Pena, L. Bolge (both LDEO), W. Buckley (USC) for their help in the lab and R.A. Mills for valuable discussions. The very constructive suggestions of the two reviewers Dr. Kazuyo Tachikawa and Dr. Hiroshi Amakawa and editor Dr. Johan Schijf improved this paper substantially. The research was funded by a collaborative NSF grant OCE09-27241 (UH), −28409 (LDEO), and−26981 (USC). This is LDEO contribution number 8186.

REFERENCES

Arsouze, T., Dutay, J.-C., Lacan, F., and Jeandel, C. (2009). Reconstructing the Nd oceanic cycle using a coupled dynamical–biogeochemical model. *Biogeosciences* 6, 2829–2846. doi: 10.5194/bg-6-2829-2009

Arsouze, T., Dutay, J., Lacan, F., and Jeandel, C. (2007). Modeling the neodymium isotopic composition with a global ocean circulation model. *Chem. Geol.* 239, 165–177. doi: 10.1016/j.chemgeo.2006.12.006

Basak, C., Pahnke, K., Frank, M., Lamy, F., and Gersonde, R. (2015). Neodymium isotopic characterization of Ross Sea Bottom Water and its advection through the southern South Pacific. *Earth Planet. Sci. Lett.* 1, 211–221. doi: 10.1016/j.epsl.2015.03.011

Behrens, M. K., Muratli, J., Pradoux, C., Wu, Y., Böning, P., Brumsack, H. J., et al. (2016). Rapid and precise analysis of rare earth elements in small volumes of seawater-Method and intercomparison. *Mar. Chem.* 186, 110–120. doi: 10.1016/j.marchem.2016.08.006

Carter, P., Vance, D., Hillenbrand, C. D., Smith, J. A., and Shoosmith, D. R. (2012). The neodymium isotopic composition of waters masses in the eastern Pacific sector of the Southern Ocean. *Geochim. Cosmochim. Acta* 79, 41–59. doi: 10.1016/j.gca.2011.11.034

Conway, T. M., and John, S. G. (2014). Quantification of dissolved iron sources to the North Atlantic Ocean. *Nature* 511, 212–215. doi: 10.1038/nature13482

Elderfield, H., and Greaves, M. J. (1982). The rare earth elements in seawater. *Nature* 296, 214–219. doi: 10.1038/296214a0

Elderfield, H., and Schultz, A. (1996). Mid-ocean ridge hydrothermal fluxes and the chemical composition of the ocean. *Annu. Rev. Earth Planet. Sci.* 24, 191–224. doi: 10.1146/annurev.earth.24.1.191

German, C. R., Campbell, A. C., and Edmond, J. M. (1991). Hydrothermal scavenging at the Mid-Atlantic Ridge: modification of trace element dissolved fluxes. *Earth Planet. Sci. Lett.* 107, 101–114. doi: 10.1016/0012-821X(91)90047-L

German, C. R., Klinkhammer, G. P., Edmond, J. M., Mura, A., and Elderfield, H. (1990). Hydrothermal scavenging of rare-earth elements in the ocean. *Nature* 345, 516–518. doi: 10.1038/345516a0

Goldstein, S. J., and Jacobsen, S. B. (1987). The Nd and Sr isotopic systematics of river-water dissolved material: implications for the sources of Nd and Sr in seawater. *Chem. Geol. Isot. Geosci. Sect.* 66, 245–272. doi: 10.1016/0168-9622(87)90045-5

Goldstein, S. L., and Hemming, S. R. (2003). "Long-lived isotopic tracers in oceanography, paleoceanography, and ice-sheet dynamics," in *Treatise on Geochemistry: The Oceans and Marine Geochemistry*, eds H. D. Holland, K. Turekian, and H. Elderfield (Pergamon: Oxford), 453–489.

Goto, S., Kinoshita, M., Schultz, A., and Von Herzen, R. P. (2003). Estimate of heat flux and its temporal variation at the TAG hydrothermal mound, Mid-Atlantic Ridge 26°N. *J. Geophys. Res. Solid Earth* 108, 1–14. doi: 10.1029/2001JB000703

Grasse, P., Stichel, T., Stumpf, R., Stramma, L., and Frank, M. (2012). The distribution of neodymium isotopes and concentrations in the Eastern Equatorial Pacific: water mass advection versus particle exchange. *Earth Planet. Sci. Lett.* 353–354, 198–207. doi: 10.1016/j.epsl.2012.07.044

Hatta, M., Measures, C. I., Wu, J., Roshan, S., Fitzsimmons, J. N., Sedwick, P., et al. (2015). An overview of dissolved Fe and Mn distributions during the 2010–2011 U.S. GEOTRACES north Atlantic cruises: GEOTRACES GA03. *Deep Sea Res. II Top. Stud. Oceanogr.* 116, 117–129. doi: 10.1016/j.dsr2.2014.07.005

Jacobsen, S. B., and Wasserburg, G. J. (1980). Sm-Nd isotopic evolution of chondrites. *Earth Planet. Sci. Lett.* 50, 139–155. doi: 10.1016/0012-821X(80)90125-9

Jeandel, C., Delattre, H., Grenier, M., Pradoux, C., and Lacan, F. (2013). Rare earth element concentrations and Nd isotopes in the Southeast Pacific Ocean. *Geochem. Geophys. Geosyst.* 14, 328–341. doi: 10.1029/2012GC004309

Jeandel, C., and Oelkers, E. H. (2015). The influence of terrigenous particulate material dissolution on ocean chemistry and global element cycles. *Chem. Geol.* 395, 50–66. doi: 10.1016/j.chemgeo.2014.12.001

Jenkins, W. J., Lott, D. E., Longworth, B. E., Curtice, J. M., and Cahill, K. L. (2015a). The distributions of helium isotopes and tritium along the U.S. GEOTRACES North Atlantic sections (GEOTRACES GAO3). *Deep Sea Res. II Top. Stud. Oceanogr.* 116, 21–28. doi: 10.1016/j.dsr2.2014.11.017

Jenkins, W. J., Smethie, W. M., Boyle, E. A., and Cutter, G., a. (2015b). Water mass analysis for the U.S. GEOTRACES (GA03) North Atlantic sections. *Deep Sea Res. II Top. Stud. Oceanogr.* 116, 6–20. doi: 10.1016/j.dsr2.2014.11.018

Jones, K. M., Khatiwala, S. P., Goldstein, S. L., Hemming, S. R., and van de Flierdt, T. (2008). Modeling the distribution of Nd isotopes in the oceans using an ocean general circulation model. *Earth Planet. Sci. Lett.* 272, 610–619. doi: 10.1016/j.epsl.2008.05.027

Klinkhammer, G., Elderfield, H., and Hudson, A. (1983). Rare earth elements in seawater near hydrothermal vents. *Nature* 305, 185–188. doi: 10.1038/305185a0

Klunder, M. B., Laan, P., Middag, R., De Baar, H. J. W., and van Ooijen, J. C. (2011). Dissolved iron in the Southern Ocean (Atlantic sector). *Deep Sea Res. II Top. Stud. Oceanogr.* 58, 2678–2694. doi: 10.1016/j.dsr2.2010.10.042

Lacan, F., and Jeandel, C. (2001). Tracing Papua New Guinea imprint on the central Equatorial Pacific Ocean using neodymium isotopic compositions and Rare Earth Element patterns. *Earth Planet. Sci. Lett.* 186, 497–512. doi: 10.1016/S0012-821X(01)00263-1

Lacan, F., and Jeandel, C. (2005). Neodymium isotopes as a new tool for quantifying exchange fluxes at the continent–ocean interface. *Earth Planet. Sci. Lett.* 232, 245–257. doi: 10.1016/j.epsl.2005.01.004

Lambelet, M., van de Flierdt, T., Crocket, K., Rehkämper, M., Kreissig, K., Coles, B., et al. (2016). Neodymium isotopic composition and concentration in the western North Atlantic Ocean: results from the GEOTRACES GA02 section. *Geochim. Cosmochim. Acta* 177, 1–29. doi: 10.1016/j.gca.2015.12.019

Mahowald, N. M., Baker, A. R., Bergametti, G., Brooks, N., Duce, R. A., Jickells, T. D., et al. (2005). Atmospheric global dust cycle and iron inputs to the ocean. *Global Biogeochem. Cycles* 19:GB4025. doi: 10.1029/2004GB002402

Middag, R., de Baar, H. J. W., Laan, P., Cai, P. H., and van Ooijen, J. C. (2010). Dissolved manganese in the Atlantic sector of the Southern Ocean. *Deep Sea Res. II Top. Stud. Oceanogr.* 58, 2661–2677. doi: 10.1016/j.dsr2.2010.10.043

Mills, R. A., Wells, D. M., and Roberts, S. (2001). Genesis of ferromanganese crusts from the TAG hydrothermal field. *Chem. Geol.* 176, 283–293. doi: 10.1016/S0009-2541(00)00404-6

Ohnemus, D. C., and Lam, P. J. (2015). Cycling of lithogenic marine particles in the US GEOTRACES North Atlantic transect. *Deep Sea Res. II Top. Stud. Oceanogr.* 116, 283–302. doi: 10.1016/j.dsr2.2014.11.019

Pahnke, K., van de Flierdt, T., Jones, K. M., Lambelet, M., Hemming, S. R., and Goldstein, S. L. (2012). GEOTRACES intercalibration of neodymium isotopes and rare earth element concentrations in seawater and suspended particles. Part 2: systematic tests and baseline profiles. *Limnol. Oceanogr. Methods* 10, 252–269. doi: 10.4319/lom.2012.10.252

Pena, L. D., and Goldstein, S. L. (2014). Thermohaline circulation crisis and impacts during the mid-Pleistocene transition. *Science* 345, 318–322. doi: 10.1126/science.1249770

Piepgras, D. J., and Wasserburg, G. J. (1982). Isotopic composition of neodymium in waters from the drake passage. *Science* 217, 207–214. doi: 10.1126/science.217.4556.207

Piotrowski, A. M., Goldstein, S. L., Hemming, S. R., and Fairbanks, R. G. (2004). Intensification and variability of ocean thermohaline circulation through the last deglaciation. *Earth Planet. Sci. Lett.* 225, 205–220. doi: 10.1016/j.epsl.2004.06.002

Rempfer, J., Stocker, T. F., Joos, F., Dutay, J.-C., and Siddall, M. (2011). Modelling Nd-isotopes with a coarse resolution ocean circulation model: sensitivities to model parameters and source/sink distributions. *Geochim. Cosmochim. Acta* 75, 5927–5950. doi: 10.1016/j.gca.2011.07.044

Resing, J. A., Sedwick, P. N., German, C. R., Jenkins, W. J., Moffett, J. W., Sohst, B. M., et al. (2015). Basin-scale transport of hydrothermal dissolved metals across the South Pacific Ocean. *Nature* 523, 200–203. doi: 10.1038/nature 14577

Rousseau, T. C., Sonke, J. E., Chmeleff, J., van Beek, P., Souhaut, M., Boaventura, G., et al. (2015). Rapid neodymium release to marine waters from lithogenic sediments in the Amazon estuary. *Nat. Commun.* 6, 7592. doi: 10.1038/ncomms8592

Schlitzer, R. (2016a). *Ocean Data View*. Available online at: http://odv.awi.de.

Schlitzer, R. (2016b). Quantifying He fluxes from the mantle using multi-tracer data assimilation. *Philos. Trans. R. Soc. A Math. Phys. Eng. Sci.* 374, 20150288. doi: 10.1098/rsta.2015.0288

Siddall, M., Khatiwala, S., van de Flierdt, T., Jones, K., Goldstein, S. L., Hemming, S., et al. (2008). Towards explaining the Nd paradox using reversible scavenging in an ocean general circulation model. *Earth Planet. Sci. Lett.* 274, 448–461. doi: 10.1016/j.epsl.2008.07.044

Stein, C. A., Stein, S., and Pelayo, A. M. (2013). "Heat Flow and Hydrothermal Circulation," in *Seafloor Hydrothermal Systems: Physical, Chemical, Biological, and Geological Interactions*, eds S. E. Humphris, R. A. Zierenberg, L. S. Mullineaux, and R. E. Thomson (Washington, DC: American Geophysical Union), 425–445.

Stichel, T., Frank, M., Rickli, J., and Haley, B. A. (2012). The hafnium and neodymium isotope composition of seawater in the Atlantic sector of the Southern Ocean. *Earth Planet. Sci. Lett.* 317–318, 282–294. doi: 10.1016/j.epsl.2011.11.025

Stichel, T., Hartman, A. E., Duggan, B., Goldstein, S. L., Scher, H., and Pahnke, K. (2015). Separating biogeochemical cycling of neodymium from water mass mixing in the Eastern North Atlantic. *Earth Planet. Sci. Lett.* 412, 245–260. doi: 10.1016/j.epsl.2014.12.008

Tachikawa, K., Athias, V., and Jeandel, C. (2003). Neodymium budget in the modern ocean and paleo-oceanographic implications. *J. Geophys. Res.* 108, 3254. doi: 10.1029/1999JC000285

Tachikawa, K., Jeandel, C., and Roy-Barman, M. (1999). A new approach to the Nd residence time in the ocean: the role of atmospheric inputs. *Earth Planet. Sci. Lett.* 170, 433–446. doi: 10.1016/S0012-821X(99)00127-2

Tanaka, T., Togashi, S., Kamioka, H., Amakawa, H., Kagami, H., Hamamoto, T., et al. (2000). JNdi-1: a neodymium isotopic reference in consistency with LaJolla neodymium. *Chem. Geol.* 168, 279–281. doi: 10.1016/S0009-2541(00)00198-4

Taylor, S. R., and McLennan, S. M. (1985). *The Continental Crust: Its Composition and Evolution*. Malden, MA: Blackwell.

Zheng, X. Y., Plancherel, Y., Saito, M. A., Scott, P. M., and Henderson, G. M. (2016). Rare earth elements (REEs) in the tropical South Atlantic and quantitative deconvolution of their non-conservative behavior. *Geochim. Cosmochim. Acta* 177, 217–237. doi: 10.1016/j.gca.2016.01.018

Conflict of Interest Statement: The authors declare that the research was conducted in the absence of any commercial or financial relationships that could be construed as a potential conflict of interest.